Astron. Astrophys. 333, 1001–1006 (1998)

ASTRONOMY AND ASTROPHYSICS

Kelvin-Helmholtz instabilities in stellar jets

IV. On the origin of the emission knots

M. Micono[1], **S. Massaglia**[1], **G. Bodo**[2], **P. Rossi**[2], **and A. Ferrari**[1,2]

[1] Dipartimento di Fisica Generale dell'Università, Via Pietro Giuria 1, I-10125 Torino, Italy (e-mail: surname@ph.unito.it)
[2] Osservatorio Astronomico di Torino, I-10025 Pino Torinese, Italy (e-mail: surname@to.astro.it)

Received 1 October 1997 / Accepted 2 January 1998

Abstract. We discuss the spatial evolution into biconical shocks of axisymmetric perturbations in supersonic jets subject to non-equilibrium radiative losses. Our aim is to interpret the origin of the knots, observed along many jets in Young Stellar Objects (YSOs), in terms of shocks originated by Kelvin-Helmholtz modes. In this scheme, we find that the $[SII]/H_\alpha$ line intensity ratios and the mean intra-knot spacing result connected to each other, and we show the evolution of the shock morphologies as a consequence of shock merging effects. From the numerical calculations we also obtain the knot proper motion velocities and the line flux behavior along the jet and make comparisons with the observations.

Key words: hydrodynamics – instabilities – ISM: jets and outflows – stars: premain sequence

1. Introduction

High spatial resolution observations of jets from young stellar objects (YSOs), performed by ground based telescopes and recently by the WFPC2 on-board of the Hubble Space Telescope (see Ray 1996), have revealed the finest details of the complex morphological structures that characterize these objects and, in particular, of the emission knots located along the jets. The origin of these knots, that are clearly visible in many objects such as HH34 (Bührke, Mundt & Ray 1988; Raga & Mateo 1988; Reipurth & Heathcote 1992; Eislöffel & Mundt 1992), and HH111 (Reipurth 1989; Reipurth, Raga & Heathcote 1992; Morse et al. 1993a) is an important issue because determining the mechanism that leads to their formation would allow a leap forward in the understanding of the nature of YSO jets, since the physical parameters of the flow could be constrained opening a window on the hidden region where the jet origin takes place actually.

Concerning the problem of the origin of the emission knots, it has been subject of many investigations during the last years. Two different interpretations have been proposed, namely: Bührke et al. (1988) suggested nonlinearly evolved Kelvin-Helmholtz instabilities as responsible for the formation and growth of perturbations into shocks, as has been later confirmed by the numerical calculation of Bodo et al. (1994, 1995), Paper I and Paper II); an alternative explanation was proposed by Raga et al. 1990 in terms of internal working surfaces that form in the jet as a consequence of variations in the jet ejection velocity (see also Kofman & Raga 1992; Raga & Kofman 1992; Raga & Cantò 1995; Hartigan & Raymond 1993; Biro & Raga 1994; Stone & Norman 1993a, 1993b).

Herbig-Haro jets therefore pose two main problems: i) they survive instabilities for distances as large as a thousand jet radii, and ii) the displayed emission knots require interpretation. The former problem was discussed, in the 2-D cylindrically symmetric limit, by Bodo et al. (1994, 1995) and Rossi et al. (1997) (see also the companion Paper III, Micono et al. 1997) who have shown that radiative losses may drastically reduce the nonlinear growth of Kelvin-Helmholtz instabilities as far as jet momentum transfer from the jet to the ambient medium is concerned, and therefore increase the jet capability to survive instabilities. Stone, Xu & Hardee (1997) have recently addressed the same problem for asymmetric modes in a slab jet and discussed the effects of different cooling and heating functions.

In this paper we study the spatial evolution of symmetric perturbations in a two-dimensional cylindrical geometry and in the presence of non-equilibrium radiative losses, and we then apply the results to stellar jets in order to interpret the origin of their emission knots, pointing out the main differences between the present scheme and the alternative internal working surfaces (IWSs) picture. We discuss also how observations can help to discriminate between these two interpretations.

The plan of the paper is the following: In the next section (Sect. 2), we summarize the observational constraints, Sect. 3 is devoted to the computational results; astrophysical applications and the conclusions are given in Sect. 4.

2. Observational constraints

For the general properties of knots we mainly refer to the HH34 and HH111 jets (see e.g. Bührke et al. (1988), Cohen & Jones (1987), Eislöffel & Mundt (1992), Heathcote & Reipurth (1992), Morse et al. (1993a)), that have been observed with the utmost detail (see Table 1 for a summary). Spectroscopical data

Send offprint requests to: S. Massaglia

Table 1. Observational constraints for jets in HH34 and HH111

	HH34	HH111
$L_{\rm knot}$ $(\times 10^{17}$ cm)	1.4 [a]	3.0 [b]
$L_{\rm gap}$ $(\times 10^{17}$ cm)	0.4 [a]	1.0
$L_{\rm tot}/L_{\rm knot}$	1.3	1.3
$L_{\rm knot}/L_{\rm gap}$	3.3	3.0
Number of knots	10 - 13 [a]	10 - 13 [b]
Jet's diameter (knot width) $(\times 10^{15}$ cm)	4.7 [a]	5.5 [b]
Knot separation $(\times 10^{16}$ cm)	0.8 - 1.7 [a]	3.0 [c]
Age (yr)	2,800 [d]	800 [c]
Age (yr)	2,800 [d]	800 [c]
Electron density $(\times$ cm$^{-3})$	1,000 [a] - 3,000 [c]	1,500 [b] - 5,000 [c]
Jet velocity (km s^{-1})	250 - 400 [e]	300 - 400 [f]
Knot pattern speed (km s^{-1})	100 - 300 [e]	300 [f]

[a] Bührke et al. (1988) [b] Reipurth (1989) [c] Morse et al. (1993a) [d] Mundt et al. (1987) [e] Eislöffel & Mundt (1992) [f] Reipurth et al. (1992)

taken at different epochs lead to somewhat different results that may imply a degree of variability in the sources; however the relevant morphological, spectral and kinematical features can be summarized as follows:

1. These objects show one-sided jets displaying a chain (10-13) of quasi-equally spaced emission knots, starting from few jet radii from the central YSO ($\sim 10''$) up to $\sim 50''-70''$; in both cases the farthest knot ('O' in HH34 and 'P' in HH111, in Morse et al. 1993a) appears more detached and shows a distinct, wide 'bow-shock like' form. Where the instrument resolution suffices, all knots show the apex in the forward direction (Ray et al. 1996), indicating a common 'bow-shock like' shape.
2. A region of very low emission (a 'gap') is present in HH34 and HH111 between the central source and the first knot. This is also true for the jet of HH1/2, but perhaps due to a reflection nebula (Reipurth et al. 1993). HH30 instead shows intense emission right from the beginning then a decline (see Lopez et al. 1995, Mundt et al. 1990).
3. The intensity in the two prominent emission lines, H_α and $[SII]$, typically increases along the jet from the first knot, reaches a maximum in the middle of the chain and then decreases.
4. The line intensity ratio $[SII]/H_\alpha$ shows a similar behavior, but Cohen & Jones (1987) find a higher value in knot 'O' of HH34 with respect to Morse et al. (1993a) (variability?).
5. The electronic density grows with the distance from the origin, attains a maximum value of $\sim 1,000 - 3,000$ cm^{-3}, then decreases.
6. Measures of knots proper motions in HH34 show *tangential* (projected) velocities that increase with distance along the jet from ~ 100 to ~ 400 km s^{-1}. Estimates of the real knot pattern and jet velocities, i.e. disentangled from projection effects, have been attempted by Eislöffel & Mundt (1992) who found a knot pattern speed to jet speed ratio again increasing steadily with distance from ~ 0.5 to ~ 1.
7. The intra-knot spacing is larger, by a factor of $\sim 1.5-2$, in HH111 with respect to HH34, and the the ratio $[SII]/H_\alpha$ is smaller in the former by a similar amount. Therefore, whatever physical mechanism is proposed for the origin of knots, this must agree, at least qualitatively, with the above constraints.

3. Physical parameters and results

The calculations have been carried out in the scheme described in Paper III for the nonlinear evolution of axisymmetric pinching (body) modes for a cylindrical jet. We have set, at $t = 0$, the jet Mach number $M = 10, 15$ and the density ratio $\nu = 1$. In order to set the remaining parameters, T_0 and $n_0 a$, we recall from Paper II that a choice of $T_0 = 10,000$ K yields post-shock temperatures $\sim 20,000 - 30,000$ K, consistent with the low excitation spectra observed. We recall also that since the initial cooling time is large with respect to the dynamical time scale, choices of T_0 that differ up to 40% have shown in tests calculations to have very little effect on the nonlinear evolution of the instability. Concerning the choice of $n_0 a$, observations of HH34 and HH111 are consistent with jet radii $\sim 10^{15}$ cm and particle density $\sim 10^2 - 10^3$ cm^{-3} (Bürkhe et al. 1988, Morse et al 1993a). We have therefore adopted for the column density $n_0 a = 10^{18}$ cm^{-2}; this choice implies for the jet a mass flux $\approx 10^{-10} \times a_{15} M$ M$_\odot$ yr^{-1} and a momentum flux $\approx 10^{-9} \times a_{15} M^2$ M$_\odot$ km s^{-1} yr^{-1}, with $a_{15} = a/(10^{15}$ cm).

In Fig. 1 we show a contour plot of the morphology of the $[SII]$ emission flux, for $M = 10$, at the time when the train of shocks has reached a distance from the origin corresponding to about 400 radii. The results for $M = 15$ yield similar morphologies. We note however that the general morphology is weakly dependent on the particular time chosen, as can be seen, for this set of parameters, in Fig. 1a,b ($t = 38.9$ (Fig. 1a) and $t = 47.3$ (Fig. 1b). In this figure we show also the details of the morphology of the leading shock, with a clear bow-like form, and of preceding ones (i.e. at smaller z) that appear to have a more compact structure. The line fluxes are obtained by integrating the emissivity along the line-of-sight under the hypothesis that this is perpendicular to the jet longitudinal axis. From Fig. 1 we see that one of the leading shocks, being a result of shock merging processes, is somewhat more distant from the preceding one, is wider and has a distinct bow-shock like morphology. The knots result quasi-equally spaced, with mean intra-knot distance of $\sim 3 - 6$ jet diameters, and with an initial gap whose length partly depends on the amplitude of the initial perturbation imposed perpendicularly to the equilibrium velocity V_0 ($= 0.1 V_0$ in the present case). We note also that the shocks most distant from the source weaken with time (compare Fig. 1a and b).

The spectral and kinematical characteristics of the shocks resulting from K-H instability are shown in Fig. 2 where we plot, at the time $t = 38.9$ and for $M = 10$, the on-axis behavior against z of the electron density $n_{\rm e}$ in units of the initial density n_0 (panel a) and the fluxes of $[SII]$ (panel b) and H_α (panel c); in panel d) we plot the flux ratio $[SII]/H_\alpha$, obtained averaging

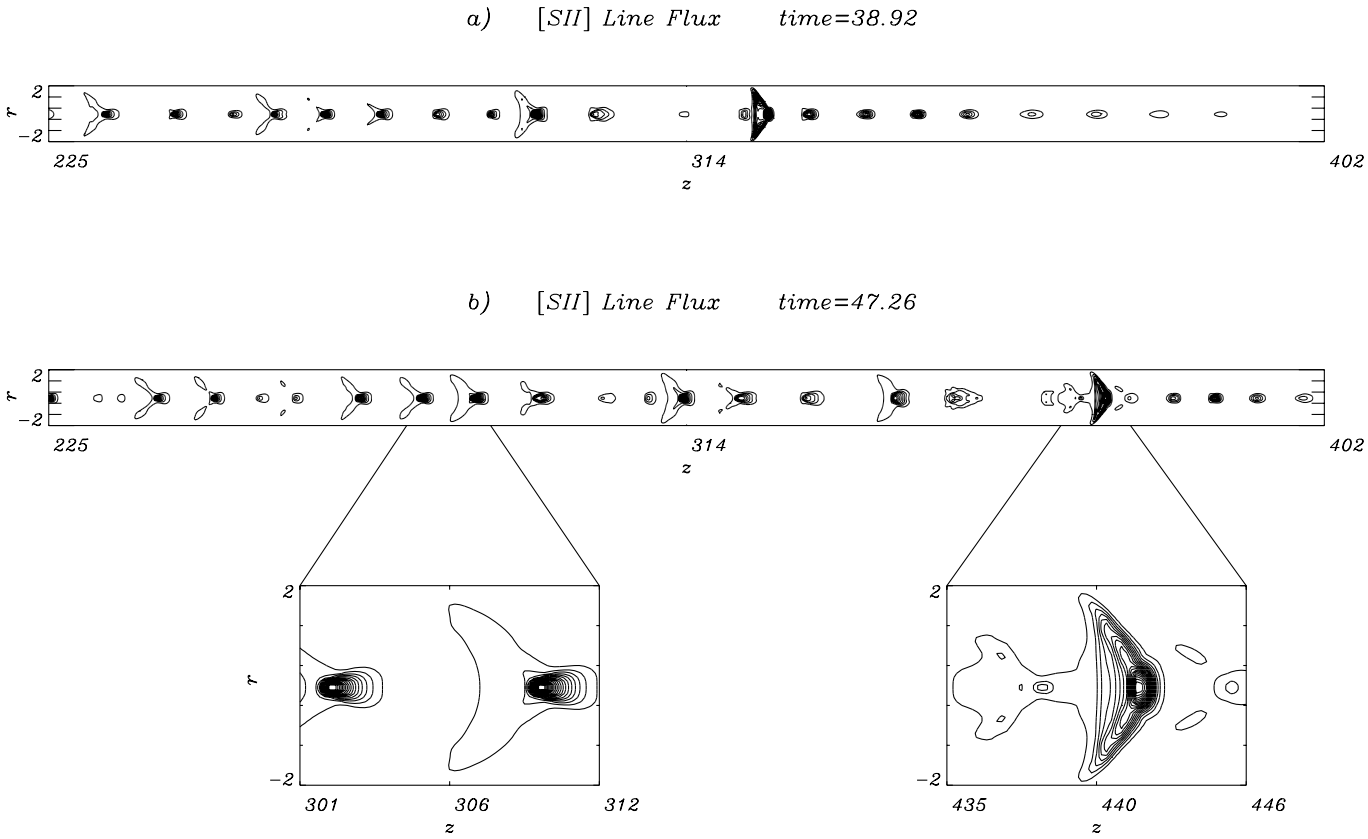

Fig. 1a and b Contour plot of the $[SII]$ emission flux spatial distribution for $M = 10$ and $t = 38.9$ (panel **a**) and $t = 47.3$ (panel **b**). Distances are expressed in units of the initial jet radius a and fluxes in units of the maximum flux

the fluxes over the emission volume of each shock, and in panel e) we show the shock pattern speeds $\xi = v_{\rm knot}/v_{\rm jet}$. As a comparison, we show in Fig. 3 the behavior of the same quantities of Fig. 2 but for $M = 15$ and at time $t = 35$. In both cases of $M = 10, 15$ the ionization fraction attains maximum values that do not exceed $\sim 3\%$, and the different shock strengths yield values of $n_{\rm e}$ reaching $\approx 0.25 n_0$ (Fig. 2a) and $\approx 0.8 n_0$ (Fig. 3a), respectively for $M = 10$ and $M = 15$. Figs. 2b,c and 3b,c show how the flux in the two lines increases, reaches a maximum and then decreases, in qualitative agreement with observations; from Figs. 2d and 3d we notice also that the line ratio attains a high value for the leading, widest shock. A further comparison of Fig. 2 with Fig. 3 show in the latter case wider initial gap and intra-shock spacings, and lower values of the $[SII]/H_\alpha$ ratio (Figs. 2d and 3d), consistently with the increasing of strength and excitation level of the shocks at a higher Mach number. Finally Figs. 2e and 3e show that the proper motions of knots increase with distance from the origin from $\xi \sim 0.4$ up to 0.8, in the case of $M = 10$, and from 0.5 up to 0.7, for $M = 15$. These results are in good qualitative agreement with the findings of Eislöffel & Mundt (1992) for HH34. We have taken Figs. 2 and 3 as representative snapshots of typical morphologies; in fact, calculations show that the shock train, after a time scale depending on the physical parameters, reaches a asymptotic configuration that remains quasi-steady and simply shifts forward.

About the possibility of shock merging effects, that lead to bow-shock like features, we note that the condition for these processes to set in is that, locally, a shock at larger z must have proper motion smaller than the following one,i.e. at smaller z (see the discussion in the companion Paper III). Looking at Figs. 2e and 3e we can see that this condition can be verified in several positions along the jet, therefore one may expect that bow-shock like knots, originated by K-H modes, can be a more common feature than actually shown in our calculations, limited in time. We remark finally the internal consistency between the increasing of shock pattern motions with distance z along the jet (Figs. 2e and 3e), which should give a lower shock strength, and the increasing of the $[SII]/H_\alpha$ ratio (Figs. 2d and 3d).

3.1. Discussion

In Table 2 we list the main results of our model for $M = 10, 15, 30$ (the reader should make comparisons with observations of HH34 and HH111 in Table 1).

We leave distances and densities in units of a and n_3, with $n_3 = n_0/1000\,{\rm cm}^{-3}$, bearing in mind that the values must obey $n_0 a = 10^{18}\ {\rm cm}^{-2}$. In Table 2, the results for $M = 10, 15$ are in general agreement with observations; setting for a the values of HH34 and HH111, the major discrepancies are: i) the length of the initial invisible part of the jet (the 'gap') that is larger by a factor of ~ 3 with respect to observations, ii) the widths

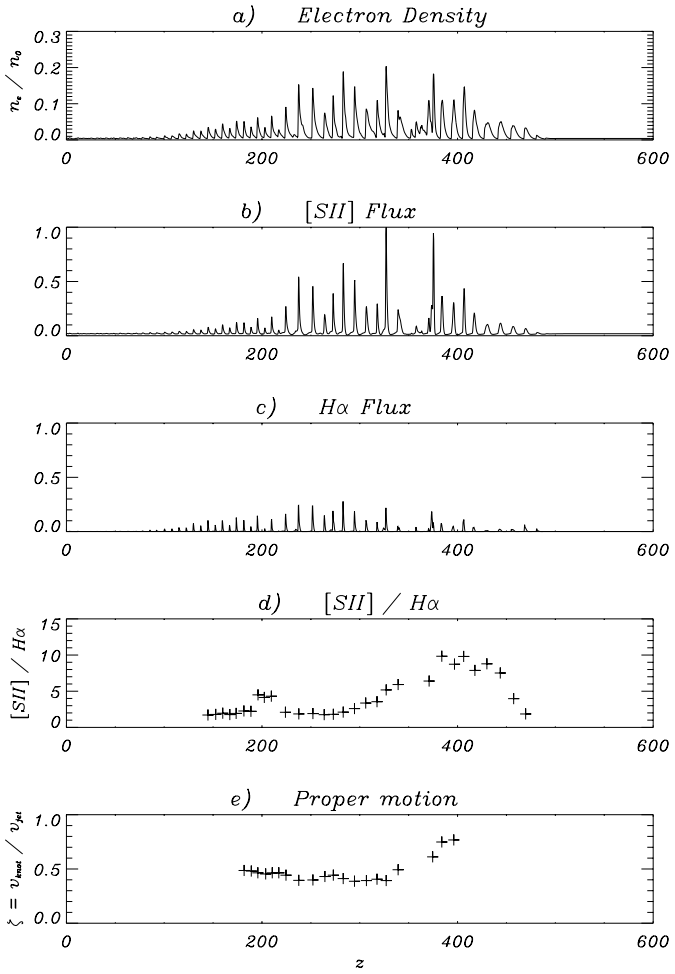

Fig. 2a–e On-axis behavior of the electron density $n_{\rm e}/n_0$ (panel **a**), line fluxes of $[SII]$ (panel **b**) in units of the maximum flux, H_α (panel **c**) in units of the maximum $[SII]$ flux, of the ratio $[SII]/H_\alpha$ (panel **d**), and of the shock pattern speeds $\xi = v_{\rm knot}/v_{\rm jet}$ (panel **e**) against z for $M = 10$ and $t = 38.9$

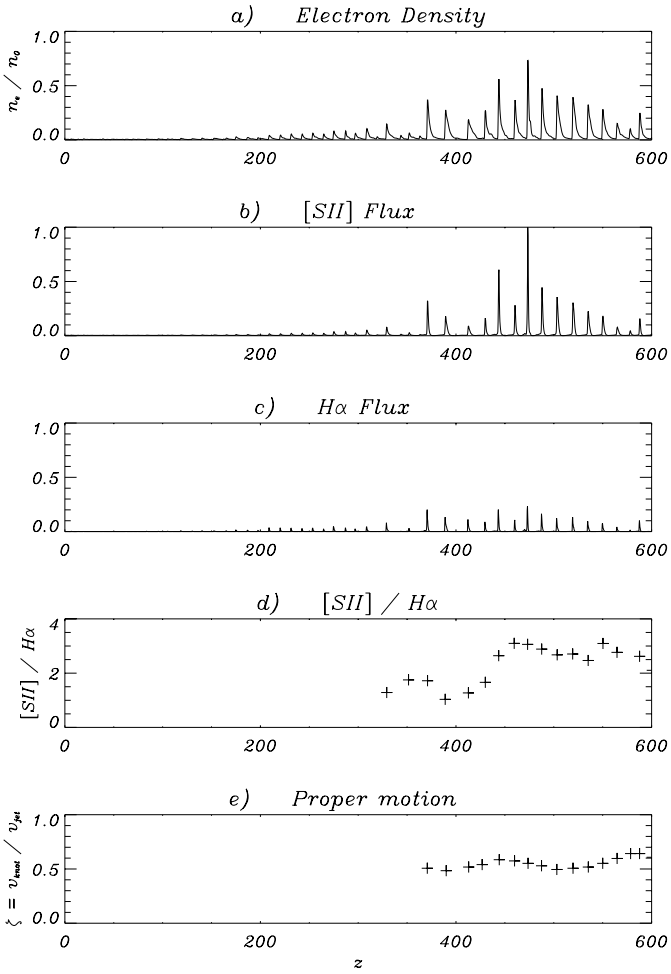

Fig. 3a–e The same as in Fig. 2, but for $M = 15$ and $t = 35$

Table 2. Model results, to be compared with Table 1

	$M = 10$	$M = 15$	$M = 30$
$L_{\rm knot}$ ($\times 10^{17}$ cm)	2.25 a_{15}	2.75 a_{15}	?
$L_{\rm gap}$ ($\times 10^{17}$ cm)	2.0 a_{15}	3.5 a_{15}	4.5 a_{15}
$L_{\rm tot}/L_{\rm knot}$	1.9	2.3	?
$L_{\rm knot}/L_{\rm gap}$	1.1	0.8	?
Number of knots	12 - 18	10 - 15	?
Knot width ($\times 10^{15}$ cm)	2.0 a_{15}	2.0 a_{15}	2.0 a_{15}
Knot separation ($\times 10^{16}$ cm)	1.25 a_{15}	1.75 a_{15}	3.1 a_{15}
Age (yr)	1,350 a_{15}	1,220 a_{15}	?
Electron density $n_{\rm e}$ ($\times$ cm^{-3})	240 n_3	730 n_3	370 n_3
Jet velocity $v_{\rm jet}$ (km s^{-1})	120	180	360
Knot speed $v_{\rm knot}$ (km s^{-1})	50 - 100	100 - 140	110 - 220

of the knots in $[SII]$ tend to be smaller by a similar factor, and iii) the post-shock electron densities are smaller than the observed values, especially in the case $M = 10$, by a factor ~ 4. However, being the choice of the set of parameters by no means unique, one can expect, at best, only a broad agreement from the comparison with observations. What is important to stress is the trend brought about by the variation of the Mach number, i.e. higher values of M cause an increase of the intra-knot spacing and a decrease of the $[SII]/H_\alpha$ ratio. Also the temporal evolution plays a role, increasing the relative length of the visible part of the jet (see Fig. 1).

Observations indicate jet velocities $\sim 200 - 400$ km s^{-1}, implying $M > 20$. Unfortunately, our capability of carrying out calculations with $M > 15$, on the same grid (2500×248), was greatly hampered by the growing size of the integration domain. In order to gain some insight on the behavior of the instability at different Mach numbers we have carried out additional calculations on a coarser grid (1024×248) for $M = 5, 30$, and with a larger longitudinal size of the domain (800 jet radii). The simulation of the case $M = 30$ has been carried out up to $t = 29$, when the leading perturbation reached the right boundary; therefore we cannot represent a quasi-steady situation and in Table 2, there are missing data for this case: $L_{\rm knot}$ is larger than the computational domain, thus we cannot estimate $L_{\rm tot}/L_{\rm knot}$, $L_{\rm knot}/L_{\rm gap}$, and the knot number; the age of the jet is also missing and the electron density is, quite likely,

severely underestimated. The remaining quantities: $L_{\rm gap}$, knot width and separation, jet velocity and knot speed are instead reasonably well defined by the simulation.

We recall that we defined M as the ratio of the jet velocity *with respect to the external medium* to the internal sound speed, and that is reported in Table 2. Observations of shock velocities in bow-shocks (Morse et al. 1992, 1993b, 1994) show values lower than those consistent with the measured proper motions of the bow-shocks themselves. This may suggest that the pre-shock ambient medium is not steady with respect to the central source, but may be drifting along the jet due to, perhaps, the effect of previous outburst of the source, thus lowering the actual velocity jump jet-to-ambient and the effective Mach number. In particular, Morse et al. (1992) found for HH34 a velocity of the pre-shock medium, at the bow-shock, $\sim 150\ {\rm km\ s^{-1}}$, and for HH111 $\sim 300\ {\rm km\ s^{-1}}$ (Morse et al. 1993b).

Following Hardee & Norman (1988), it is possible to derive that, in the linear and adiabatic regime, this mode has a resonance frequency $\omega_{\rm R} \gtrsim \pi$ and a corresponding resonance wavelength

$$\lambda_{\rm R} \lesssim \alpha\,\pi\,\frac{M}{0.66+\sqrt{1/\nu}}\,a\,, \qquad (1)$$

where $\alpha \sim 1$ is a coefficient that depends on the geometry (Cartesian or cylindrical) and on the particular mode (symmetric or asymmetric).

The numerical results for the nonlinear evolution are reported in Fig. 4a,b. In Fig. 4a symbols represent the mean intra-knot spacing, in units of a, as a function of M and the error bars indicate the difference between maximum and minimum spacing. The dashed line shows the resonance wavelength of the fastest growing mode in the linear and adiabatic regime, according to (1), and the dot-dashed line interpolates our nonlinear results but with coefficient $\alpha = 0.5$ instead of $\alpha = 0.7 - 0.8$ of (1). In Fig. 4b we plot $[SII]/H_\alpha$ intensity ratio against M. To avoid ambiguity in the choice of a particular shock, we have selected one of the first shocks of the chain that have the advantage of being nearly of constant strength for a given M, as time elapses. The behavior of the intensity ratio is well represented by a power-law fit $[SII]/H_\alpha = M^{-3/4}$ (solid line). Therefore, in the K-H scenario, the larger is the mean intra-knot spacing the smaller must be the line ratio.

These last results show clearly how two of the main observable features of stellar jets, such as the intra-knot spacings and the line ratios, result connected if knots originate from the K-H instability, and this represents a test on the mechanisms proposed and a prediction for further observations (cf., point 7 in Sect. 2).

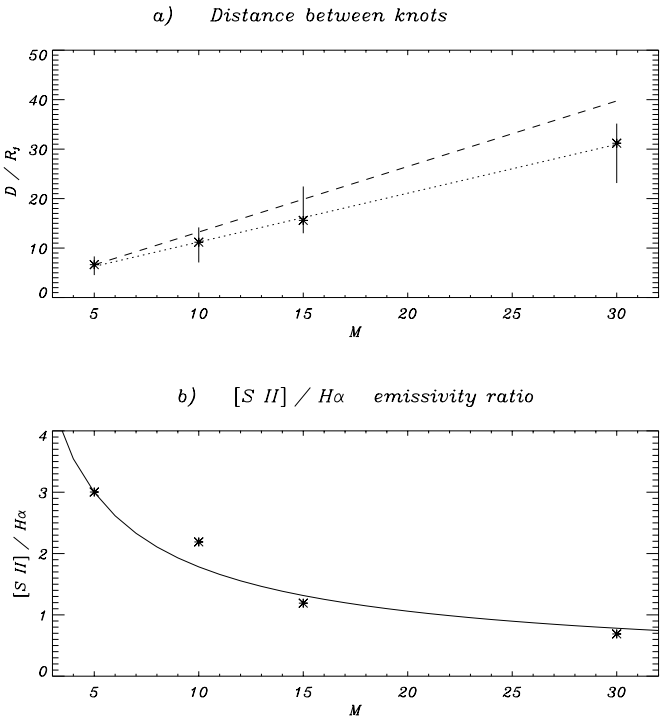

Fig. 4a and b Panel **a**: plot of the mean intra-knot spacing vs M (symbols), dashed line shows the fastest growing mode in the linear and adiabatic regime, and the dot-dashed line an interpolation of the nonlinear results; panel **b**: plot of $[SII]/H_\alpha$ vs M for one of the first shocks of the chain, the solid line is a power-law fit $[SII]/H_\alpha = M^{-3/4}$

4. Conclusions

We have applied the results obtained from the spatial nonlinear evolution of K-H modes in a cylindrical radiative jet, in order to interpret the formation of emission knots in HH jets.

The main differences between K-H and the alternative IWSs mechanisms can be summarized as follows:

1. For IWSs, the line fluxes from knots show a sudden rise and then a steady decline with distance, while for K-H they show a smooth increase followed by a slow decrease.
2. In the IWSs scenario, knots are characterized by pattern speeds very close to the jet speed while K-H mechanism produces shocks whose proper motion velocities tend to increase with distance.
3. K-H scenario predicts intra-knot spacings *and* line intensity ratios $[SII]/H_\alpha$ that depend on the jet Mach number, which is not true for IWSs scenario where they are independent each other with the former depending on the timing of successive outbursts and the latter on the amplitude of the velocity jumps.
4. Knots in HH jets displaying symmetric intra-knot spacings in jet and counter-jet, and with evidences of intrinsic differences in the respective environments, are not likely to be interpreted as results of K-H instabilities. Instead in the opposite cases, when this symmetry is missing, IWSs can hardly be responsible of the knot origin.

The K-H scenario has the basic advantage of producing morphologies directly from the hydrodynamics of the problem, works under very general conditions, and does not depend on a peculiar behavior of the source but only on the establishment of pressure balance conditions between the jet and its environment. The main problems with K-H are shock morphologies,

that only in few cases appear bow-shock like, and spatial distances within the jet are better interpreted by values of M about one half of those derived by observations of jet velocities (but not of jet-to-ambient velocity jumps).

Finally, magnetic fields may have an important impact on the phenomenology of both K-H and IWS scenarios, and the 2-D axial symmetry assumed in the calculations neglects the evolution of higher modes. Radiative 3-D calculations for the nonlinear evolution of K-H instabilities are in progress.

References

Biro S., Raga A.C., 1994, ApJ 434, 221

Bodo G., Massaglia S., Ferrari A., Trussoni E., 1994, A&A 283, 655

Bodo G., Massaglia S., Rossi P., Rosner R., Malagoli A., Ferrari A., 1995, A&A 303, 281

Bührke T., Mundt R., Ray T.P., 1988, A&A 200, 99

Cohen M., Jones B.F., 1987, ApJ 321, 846

Colella P., Woodward P.R., 1984, J. Comp. Phys. 54, 174

Gouveia Dal Pino E.M, Benz W., 1994, ApJ 435, 261

Eislöffel J., Mundt R., 1992, A&A 263, 292

Falle S., Raga A.C., 1993, MNRAS 261, 573

Hardee P.E., Norman M.L., 1988, ApJ 334, 70

Hartigan P., Raymond J., 1993, ApJ 409, 705

Hartigan P., Morse J.A., Raymond J., 1994, ApJ 436, 125

Heathcote S.R., Reipurth B., 1992, AJ 104, 2193

Kofman L., Raga A.C., 1992, ApJ 390, 359

Lopez R., Raga A.C., Riera A., Anglada G., Estalella R., 1995, MNRAS 274, 19L

Massaglia S., Rossi P., Bodo G., Ferrari A., 1996, Ap. Lett. Comm. 34, 295 (Paper I)

Micono M., Massaglia S., Bodo G., Rossi P., Ferrari A., 1997, A&A, submitted (Paper III)

Morse J.A., Hartigan P., Cecil G., Raymond J.C., Heathcote S., 1992, ApJ 399, 231

Morse J.A., Heathcote S.R., Hartigan P., Cecil G., 1993a, AJ 106, 1139

Morse J.A., Heathcote S., Cecil G., Hartigan P., Raymond J.C., 1993b, ApJ 410, 764

Morse J.A., Hartigan P., Heathcote S., Raymond J.C., Cecil G. 1994, ApJ 425, 738

Morse J.A., Hartigan P., Heathcote S., Raymond J.C., Cecil G. 1994, ApJ 425, 738

Mundt R., Brugel E.W., Bührke T., 1987, ApJ 319, 275

Mundt R., Ray T.P., Bührke T., Raga A.C., Solf J., 1990, A&A 232, 37

Payne D.G., Cohn H., 1985, ApJ 291, 655

Raga A.C., Mateo M., 1988, AJ 95, 543

Raga A.C., Cantó J., Binette L., Calvet N., 1990, ApJ 364, 601

Raga A.C., Kofman L., 1992, ApJ 386, 222

Raga A., Cantò J., 1995, Rev. Mex. Astron. Astrofis. 31, 51

Ray T.P., in: Solar and Astrophysical Magnetohydrodynamic Flows, K. Tsinganos (ed.), NATO ASI Series, 1996, p. 539

Ray T.P., Mundt R., Dyson J.E., Falle S.A.E.G., Raga A.C., 1996, ApJ 468, L103

Rees M.J., 1978, MNRAS 184, 61

Reipurth B., 1989, Nature 340, 42

Reipurth B., Heathcote S., 1992, A&A 257, 693

Reipurth B., Raga A.C., Heathcote S.R., 1992, ApJ 392, 145

Reipurth B., Heathcote S.R., Roth M., Noriega-Crespo A., Raga A.C., 1993, ApJ 408, 49L

Rossi P., Bodo G., Massaglia S., Ferrari A., 1997, A&A, **321**, 672 (Paper II)

Stone J., Norman M., 1993a, ApJ 413, 198

Stone J., Norman M., 1993b, ApJ 413, 210

Stone J.M., Xu J., Hardee, P.E., 1997, ApJ 483, 136